ChemPubSoc Europe

DOI: 10.1002/cssc.201500425

CHEMSUSCHEM Full Papers

Role of Exposed Surfaces on Zinc Oxide Nanostructures in the Catalytic Ethanol Transformation

María V. Morales,[a] Esther Asedegbega-Nieto,[a] Ana Iglesias-Juez,[b] Inmaculada Rodríguez-Ramos,[b] and Antonio Guerrero-Ruiz*[a]

For a series of nanometric ZnO materials, the relationship between their morphological and surface functionalities and their catalytic properties in the selective decomposition of ethanol to yield acetaldehyde was explored. Six ZnO solids were prepared by a microemulsion-precipitation method and the thermal decomposition of different precursors and compared with a commercial sample. All these materials were characterized intensively by XRD and SEM to obtain their morphological specificities. Additionally, surface area determinations and IR spectroscopy were used to detect differences in the surface properties. The density of acid surface sites was determined quantitatively using an isopropanol dehydration test. Based on these characterization studies and on the results of the catalytic tests, it has been established that ZnO basal surfaces seem to be responsible for the production of ethylene as a minor product as well as for secondary reactions that yield acetyl acetate. Furthermore, one specific type of exposed hydroxyl groups appears to govern the surface catalytic properties.

Introduction

Chemical conversions over solids with acidic properties have received much attention compared to the small amount of data collected for basic catalysts. However, in recent years, there has been a renewed interest in heterogeneous catalysts that have exposed surfaces with basic properties because of their good performance in some reactions of biomass transformation,[1] among others. Biomass and its derivatives provide some viable routes to alleviate the strong worldwide dependence on fossil fuels.[2] One of the major products from biomass conversion is ethanol, a commodity chemical derived from the fermentation of sugarcane or energy-rich crops such as corn.[3] Bioethanol can be the raw material to manufacture a number of chemical products.[4] An important pathway for ethanol conversion is its dehydration over acid catalysts to yield ethylene, which has received much attention in the literature.[5] However, less attention has been focused on ethanol dehydrogenation to acetaldehyde, which is favored on basic catalysts.[6] Recently, acetaldehyde has been categorized as a promising ethanol derivative from a sustainable perspective.[4] This chemical is an important intermediate in organic synthesis and is used as raw material for the production of acetic acid, acetic anhydride, ethyl acetate, butraldehyde, crotonaldehyde, pyridine, peracetic acid, vinyl acetate, and many other products.[7] Besides, acetaldehyde obtained from ethanol can be a basic reactant for subsequent condensation reactions to yield larger molecules such as 1-butanol[8] or 1,3-butadiene.[9] Industrially, acetaldehyde is mainly obtained by the direct catalytic oxidation of ethylene by the Wacker process, which produces chlorinated wastes and is energetically costly.[10] Therefore, there is a need to develop new synthetic routes and improved heterogeneous catalysts for this process.

An alternative for solid catalysts that exhibit basic properties are those derived from ZnO, which is a promising candidate for ethanol catalytic valorization.[11] ZnO materials have recently become the focus of many studies that address their use as heterogeneous catalysts for a variety of reactions. ZnO is an essential component of methanol synthesis catalysts[12] and has been suggested as a suitable catalyst for water[13] and sulfur hydride[14] dissociations, for desulfurization processes,[15] for the water gas shift reaction,[16] for CO_2 activation processes,[17] and for the conversion of maleic anhydride into 1,4-butanediol.[18] However, ZnO, as a metal oxide semiconductor, has also received much attention because of its photocatalytic properties. For instance, some studies of its application as a photocatalyst in the degradation or in complete mineralization of environmental pollutants have been presented.[19]

Pure ZnO materials crystallize in a wurtzite-type structure. Microcrystalline powder of ZnO is usually made up of hexagonal prisms, in which the (0001) and (000$\bar{1}$) polar faces are located perpendicular to the *c* axis, and the nonpolar ones, (10$\bar{1}$0) and (11$\bar{2}$0), are parallel to the [0001] axis. These surfaces are created simultaneously if the crystal is cut along a basal plane (Scheme 1).[20] Nonpolar surfaces, of which the (10$\bar{1}$0) surface is the most studied, exhibit almost equivalent amounts of Zn and O atoms and do not need to compensate any surface dipole moment. In contrast, the polar Zn-terminated (0001) surface and the O-terminated (00$\bar{0}$) surface can possess large

[a] M. V. Morales, Dr. E. Asedegbega-Nieto, Prof. A. Guerrero-Ruiz
Department Inorganic and Technical Chemistry
UNED, Facultad de Ciencias
Paseo Senda del Rey 9, 28040 Madrid (Spain)
E-mail: aguerrero@ccia.uned.es

[b] Dr. A. Iglesias-Juez, Prof. I. Rodríguez-Ramos
Instituto de Catálisis y Petroleoquímica
CSIC
C/Marie Curie 2, Cantoblanco, 28049 Madrid (Spain)

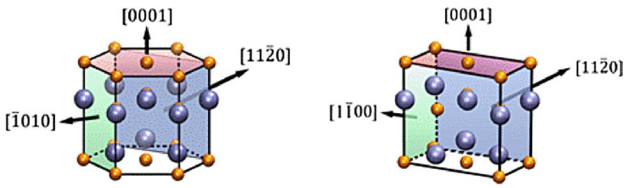

Scheme 1. Crystallographic ZnO wurtzite structure. Preferential surface orientations are displayed with colored planes and direction vectors for the hexagonal (left image) and the orthorhombic (right image) unit cells. Orange and blue spheres denote O and Zn atoms, respectively.[33]

dipole moments.[21] As ZnO exhibits a variety of morphologies, which include single-crystal surfaces,[22] thin films,[23] nanostructures,[24] and well-faceted nanoparticles,[25] with distinct polar/nonpolar facet ratios, many experimental studies have addressed this point by relating the catalytic behavior to structural factors. However, the discussion remains open to a large extent. On one hand, some research groups assign the highest catalytic activities to polar surfaces[24–26] and point out that such surfaces are the most unstable, that is, exhibit the highest surface energy, and consequently are prone to react more easily. On the other hand, others have shown that nonpolar surfaces[22] are responsible for the catalytic performance.

Surface crystalline structures are well known to be a fundamental aspect in the activity and selectivity in heterogeneous catalysis using metal oxides.[27] The surface structure sensitivity phenomenon, which implies that active sites are different from one crystalline face to another, was suggested by Boudart for metallic nanoparticles.[28] Structure sensitivity on metal oxides for oxidation reactions was demonstrated for the first time by Volta et al.[29] for propene partial oxidation to acrolein, who used a new method to prepare MoO_3 crystals with specific orientations. In the particular case of ZnO, apart from photocatalysis, there is very little data that deals with the influence of the morphology or surface properties of ZnO powders in their behavior towards chemical reactions in catalysis. Indeed, there is a lack of fundamental understanding on how these ZnO powders work under real catalytic reactions, and the aspects on which the catalytic activity and selectivity depend on surface structures are still matters of debate. In some studies, the catalytic activity of the polar surfaces was found to be higher than that of the nonpolar surfaces, such as in methanol synthesis,[30] in the decomposition of terminal alkynes, and in the decomposition of acetic and propionic acids.[31] However, most of these studies concern single crystals and/or high-vacuum conditions. It is known that the surfaces of polycrystalline ZnO particles comprise a large number of defects such as steps, edges, corners, kinks, and vacancies, which are not present on perfect single-crystal surfaces.

As mentioned above, polar surfaces on ZnO are intrinsically unstable, and different stabilization processes can occur. Examples of stabilizing processes are surface reconstruction,[32] saturation of the surface with hydroxyl groups through the adsorption of hydrogen or water,[21] and the formation of oxygen vacancies on the polar O-terminated (000$\bar{1}$) surface. The latter was proposed to play an important role in catalysis on ZnO, for example as active sites for methanol synthesis,[33] and has recently been proposed to be a pivotal factor in ethanol conversion to yield acetaldehyde and/or ethylene.[11] With respect to the surface hydroxyl groups on polar surfaces, there is also an open discussion of their role in catalysis. This is because, in many catalytic reactions, one or more reaction steps involve hydrogenation/dehydrogenation of the reaction species, likely to be performed by these surface moieties.[34] Furthermore, it is known that the presence of surface hydroxyl groups could modify the acid–base surface properties of the material. Indeed, it has been shown that in many solid bases, such as rare earth oxides[35] or hydrotalcites,[36] surface hydroxylation partially controls their reactivity.

In the present work, we explore the relationship between the ZnO morphology and the surface reactivity during the dehydrogenation of ethanol for a series of seven nanometric samples, six synthesized in the lab and one available commercially. The structural and chemical differences encountered for the different nanostructures are analyzed as a function of the specific surface planes exposed to the medium. The main characterization tools applied are surface area (S_{BET}) determination, XRD, and SEM for structural and morphological details. Diffuse reflectance infrared Fourier transform spectroscopy (DRIFTS) and catalytic tests of isopropanol dehydrogenation/dehydration are used to determine the main acid–base surface properties. The information obtained from these characterization methods is used to discuss the reactivity of the exposed facets of these polycrystalline ZnO samples in the ethanol decomposition reaction.

Results and Discussion

Some characterization results that concern the textural, structural, and morphological properties of the samples are summarized in Table 1. Although samples ZnO-E3, ZnO-E4, ZnO-ox, and ZnO-E5 have a relatively high BET surface area (20–40 m^2g^{-1}), the other three zinc oxides, ZnO-hc, ZnO-A, and ZnO-h, exhibit lower specific surface areas, less than 7 m^2g^{-1},

Table 1. S_{BET}, intensity ratio of XRD (10$\bar{1}$0)/(0002) peaks, morphological observations, range of particle sizes measured from the SEM micrographs, and average particle size calculated from the principal XRD peak of the ZnO samples.

Sample	S_{BET} [m^2g^{-1}]	(10$\bar{1}$0)/(0002)	Morphological issues[a]	Particle size[a] [nm] SEM	XRD[b]
ZnO-E3	38	0.97	brick[c]	20–200	32
ZnO-E4	35	1.06	hexagonal[c]	10–50	37
ZnO-ox	23	1.31	hexagonal disk	30–80	45
ZnO-E5	23	1.44	needle[c]	20–120	43
ZnO-h	0.8	1.27	hexagonal disk	200–1000	>100
ZnO-hc	6.7	1.27	hexagonal disk	80–200	86
ZnO-A	2.9	1.29	hexagonal prism	100–400	>100

[a] Observed by SEM. [b] Particle sizes calculated by the application of the Debye–Scherrer equation to the principal ZnO XRD peaks. [c] Studies by TEM also support these morphological observations, as reported in Refs. [20, 26]

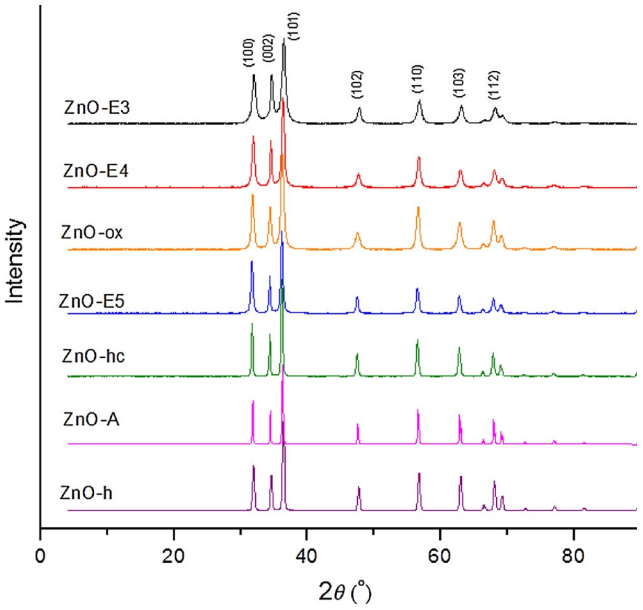

Figure 1. XRD patterns of ZnO samples.

which results in a BET surface area of close to 1 $m^2 g^{-1}$ for ZnO-h.

XRD patterns of the bulk ZnO samples are shown in Figure 1. All seven ZnO samples present the typical XRD diffraction character of the wurtzite structure according to the standardized card (JCPDS 36-1451). The main peaks at $2\theta =$ 31.8, 34.5, 36.3, 47.6, 56.6, 62.9, 66.5, 68.0, 69.2, 72.7, and 77.1° correspond to the (10), (002), (101), (102), (110), (103), (200), (112), (201), (004), and (202) crystalline planes of ZnO, respectively. If we establish the relationship between the cubic and hexagonal systems, it is found that the (100) and (002) planes correspond to the (10$\bar{1}$0) and (0002) planes of the hexagonal structure, respectively (Scheme 1). In the case of the four samples with a high specific surface (higher than 20 $m^2 g^{-1}$), it can be seen that the (10$\bar{1}$0)/(0002) intensity ratio varies from 0.97 to 1.44 (ZnO-E3 < ZnO-E4 < ZnO-ox < ZnO-E5, Table 1), which evidences a morphological variation in which the growth perpendicular to the crystallographic *c* axis is favored if this ratio is increased and, consequently, leads to an increase in the extent of basal planes at the surface, or viewed from another perspective, to a decrease of the nonpolar versus polar surface proportion. According to our XRD results, ZnO-E5 exhibits the highest basal surface extent; in other words, ZnO-E5 presents a preferred orientation in the [10$\bar{1}$0] direction that exposes basal (0001)/(000$\bar{1}$) surfaces. By contrast, ZnO-E3 has a higher proportion of nonbasal facets. Notably, the rest of the samples, ZnO-hc, ZnO-A, and ZnO-h, which have low specific surface areas, and ZnO-ox, have a very similar (10$\bar{1}$0)/(0002) intensity ratio of around 1.30, and consequently, a similar morphology is expected for these samples.

Such morphological evolution throughout our first series of samples was also studied by SEM. SEM images of the sample with the lowest (10$\bar{1}$0)/(0002) intensity ratio, ZnO-E3, show small particles between 20 and 100 nm with a brick-like morphology (Figure 2a). This corresponds to slightly elongated

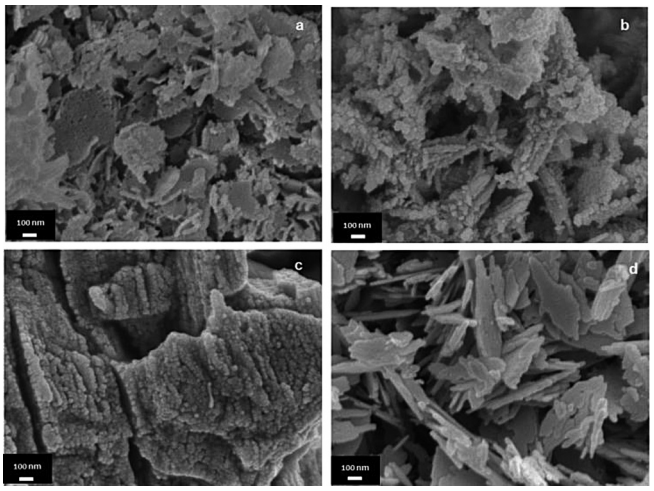

Figure 2. SEM images of the ZnO samples with different (10$\bar{1}$0)/(0002) XRD peak intensity ratios. a) ZnO-E3, b) ZnO-E4, c) ZnO-ox, and d) ZnO-E5. Scale bars correspond to 100 nm.

particles along the *c* crystallographic orientation and presents a larger contribution of nonpolar (10$\bar{1}$0) than basal (0001)/(000$\bar{1}$) plane types. ZnO-E4 exhibits poorly identifiable particle shapes by SEM (Figure 2b). Images of ZnO-ox show rounded (hexagon-like) ZnO nanoparticles with sizes around 30–80 nm (Figure 2c). For ZnO-E5, more elongated forms are shown that display some needle-like structures in which the nanostructure grows in a direction perpendicular to the crystallographic *c* axis and mainly exposes (0001)/(000$\bar{1}$) facets along the needle surface layer (Figure 2d). The SEM study of the low-surface-area samples [ZnO-h (Figure 3a), ZnO-hc (Figure 3b), and

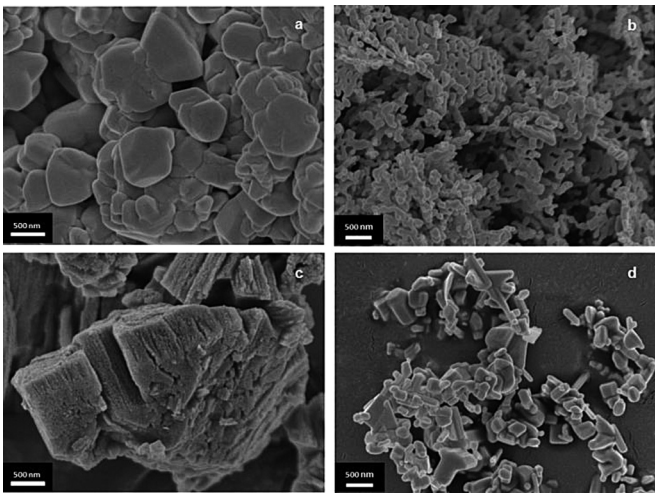

Figure 3. SEM images of the ZnO samples with similar (10$\bar{1}$0)/(0002) intensity ratios. a) ZnO-h, b) ZnO-hc, c) ZnO-ox, and d) ZnO-A. Scale bars correspond to 500 nm.

ZnO-A (Figure 3d)] and ZnO-ox (Figures 2c and 3c), which have similar (10$\bar{1}$0)/(0002) intensity ratios, reveals that these samples show a hexagonal-type morphology, which evidences a preferential exposure of the (0001)/(000$\bar{1}$) planes. This mor-

phology type is clear in the ZnO-h sample (Figure 3a), which exhibits the largest crystallite size (between 200 and 1000 nm). However, in the case of ZnO-A, SEM images also show elongated hexagonal prisms.

The particle sizes of the ZnO nanocrystals were obtained by the Scherrer method from the XRD patterns (broadening of the peaks).[37] These values are presented in Table 1 and are comparable with those obtained directly from the SEM images (Table 1). In most cases these values are on the nanometer scale, except for ZnO-A and ZnO-h, for which the particle sizes are out of the range of the application of the Scherrer equation (>100 nm). Notably, the particle size calculated is in good agreement with the surface areas measured for the samples.

SEM and XRD are physical techniques that give information on the entire material and provide morphological and structural information, whereas a surface technique such as DRIFTS allows us to explore the chemistry of the surfaces, which are clearly involved more directly in the catalytic reaction. Shape modification involves changes in the ratio of the exposed faces for both polar and nonpolar surfaces, which presumably means chemical differences because of the presence of different surface sites. DRIFTS is a powerful tool in the description of the morphology and surface ZnO nanostructures and allows the tracking of surface active sites and the identification of different types of hydroxyl groups that depend on the dominance of nonpolar or polar surfaces[20] on faceted nanoparticles.

The DRIFTS spectral region that corresponds to hydroxyl-related contributions for all ZnO samples are presented in Figure 4. The presented spectra were obtained after in situ treatments at 423 K under a dry gas flow. The spectra shown

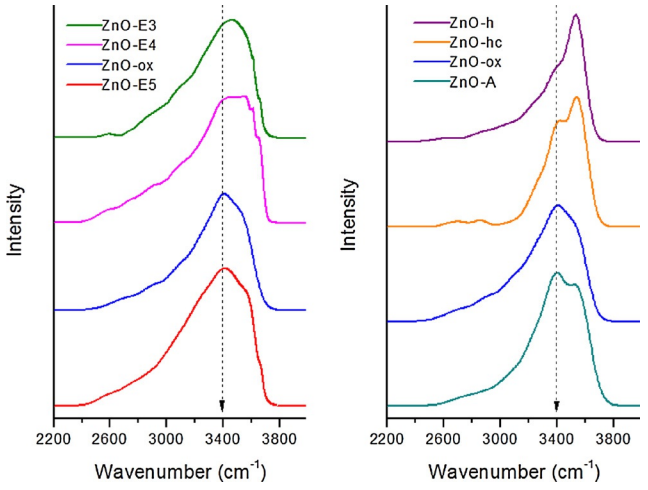

Figure 4. DRIFTS spectra in the hydroxyl region for ZnO samples with a) different and b) similar (10$\bar{1}$0)/(0002) XRD peak intensity ratios.

can be divided into four different regions defined by cutoff levels at $\tilde{\nu}\approx$3100, 3370, and 3500 cm^{-1}. The first region of low-wavenumber values contains relatively small contributions that are presumably dominated by interacting OH species as well as molecularly adsorbed water[38] on nonpolar (10$\bar{1}$0) surfaces (e.g., bands between $\tilde{\nu}$=2600 and 3100 cm^{-1}). The middle-wavenumber region (e.g., bands between $\tilde{\nu}$=3100 and 3370 cm^{-1}) contains contributions from isolated OH species on nonpolar (11$\bar{2}$0) surfaces.[38,39] This region exhibits slight variance for the four samples presented in Figure 4a. However, in the wavenumber region over $\tilde{\nu}$=3370 cm^{-1}, most significant differences were observed between these samples; a certain tendency in the peak centered at $\tilde{\nu}$=3400 cm^{-1} is appreciable and follows the intensity order: ZnO-E3<ZnO-E4<ZnO-ox<ZnO-E5. This contribution has been proposed to correspond to O_s–H species (conformation with H attached to an O surface atom) on O-terminated (000$\bar{1}$) polar surfaces.[39] The peak trend shows a clear correlation to the variation of morphology in these four samples, that is, the higher the proportion of exposed polar faces (evidenced by XRD) the greater contribution of the peak around $\tilde{\nu}$=3400 cm^{-1}. The hydroxyl groups exposed on the basal faces of the ZnO crystallites have a more acidic character than those on other surfaces. Finally, signals above $\tilde{\nu}$=3500 cm^{-1} are associated with OH groups with a more basic character and related to both basal (000$\bar{1}$) and nonpolar (10$\bar{1}$0) surfaces. Although the latter seem to be more important at higher wavenumbers, it is not possible to establish significant differences between these spectra that can be related to the structural findings (i.e., XRD).

Interestingly, DRIFTS spectra of samples with a comparable (10$\bar{1}$0)/(0002) XRD intensity ratio (ZnO-h, ZnO-hc, ZnO-ox, and ZnO-A) display significant differences (Figure 4b). These can be related qualitatively to the contribution of the peaks at $\tilde{\nu}$ ≈3400 cm^{-1}, that is, O_s–H species of moderate acidity increase in the order ZnO-h<ZnO-hc<ZnO-ox<ZnO-A. If we take into account the previous XRD and SEM results, the different proportion of this contribution cannot be ascribed to the different ratio of polar/nonpolar faces. These IR experiments indicate that the exposed O–H species are not equivalent. However, the presence of other types of hydroxyl groups, that is, exposed on the edges and kinks of the crystallites, cannot be ruled out if we consider the relatively high BET surface area of these samples. Therefore, although these ZnO materials possess similar structural characteristics, they exhibit different acid–base characters depending on the preparation treatment.

To obtain a quantitative measurement of the acidic properties for the ZnO samples with similar structural characteristics (Figure 1) and with different surface area values (Table 1), we performed isopropanol decomposition as a test reaction. This method presents the advantage of studying the solid materials under similar conditions (temperatures, flow of reactant gases, etc.) than if they are analyzed in the transformation of ethanol. In general, isopropanol is dehydrated to propylene mainly over acidic sites and dehydrogenated to acetone over basic or redox sites. These transformations occur through different mechanisms that depend on the nature of the catalysts.[40] The main results achieved with this procedure for these ZnO catalysts are collected in Table 2. Only two reaction products were obtained with our ZnO samples: acetone with selectivities higher than 97% in all cases and propylene as a minor byproduct. Clearly, these selectivities indicate that ZnO surfaces mainly expose basic sites. Furthermore, the obtained informa-

Table 2. Initial isopropanol selectivities and specific activities of the acid surface sites (5 min of reaction at 493 K).

Sample	Selectivity [%]		Acid centers
	acetone	propylene	[$\times 10^3$ µmol $m^{-2} s^{-1}$]
ZnO-h	99.1	0.9	1.71
ZnO-hc	99.0	1.0	2.15
ZnO-ox	99.0	1.0	3.46
ZnO-A	97.9	2.1	5.59

tion can be considered as quantitative, so we can obtain values related to the density of the active surface sites. We have not determined the amount of basic surface sites from isopropanol converted to acetone because these ZnO samples suffer severe deactivation under the studied reaction conditions. The reported data were measured after a short time on stream (5 min), and propylene formation, mainly over acidic sites, was used to evaluate the concentration of acidic surface sites to corroborate the DRIFTS finding of acid hydroxyl groups. Surfaces of oxide powder particles comprise a large number of defects such as steps, edges, corners, kinks, and vacancies, and particularly for samples with higher specific surface areas ($>30\ m^2 g^{-1}$), deactivation during tests is very fast. ZnO-E3, ZnO-E4, and ZnO-E5 are intrinsically unstable in the isopropanol test, which makes it impossible to obtain reproducible data. For the other ZnO samples, the density of acidic sites can be estimated easily by dividing the specific catalytic activity (µmol of $CH_3CHOHCH_3$ transformed into C_3H_6 per gram of catalyst) by the surface area of the sample, and these results are reported in Table 2. Interestingly, the order of the degree of acidity for these four samples follows the trend of the IR intensity of the acidic hydroxyl group at $\tilde{\nu} \approx 3400\ cm^{-1}$ (Figure 4b). Thus these ZnO samples with very similar structural characteristics are different if we study their acid surface properties, either by DRIFTS or by the isopropanol test.

The results of the activity tests in the ethanol reaction are summarized in Figures 5 and 6. The mass of catalyst in each experiment was adjusted in each case to work under isoconversion conditions, that is, conversions between 15 and 20% in all cases. The product distribution under these conditions reflects the specific nature of the active surface sites as it minimizes secondary reactions, although the complete limitation of the secondary reactions is rather difficult in this reaction. For all the studied catalysts, ethanol is converted mainly into acetaldehyde (selectivities of 84–94%), whereas the primary product ethylene becomes minor (selectivities lower than 8%). Some condensation products were also obtained: ethyl acetate with selectivities of 2–6% and 2-butenal (crotonaldehyde) with very low selectivities close to 1–3%. With regard to a reaction mechanism that can justify the production of a given compound, the main primary product, acetaldehyde, is obtained from the classical dehydrogenation of ethanol. According to the literature, this dehydrogenation involves the initial adsorption of ethanol on a strong acid–base pair, Zn^{2+}–O^{2-} species in our studied samples. Then, the abstraction of the adsorbed hydrogen leads to a surface ethoxy intermediate that undergoes

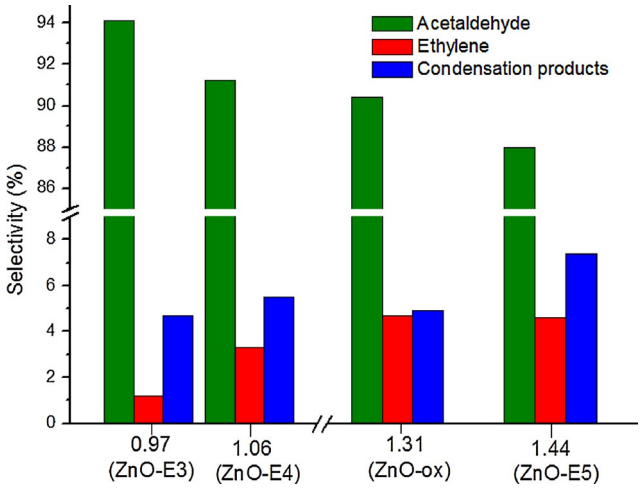

Figure 5. Selectivity results at 623 K for samples with different (10$\bar{1}$0)/(0002) XRD peak intensity ratios. The results presented correspond to average values after 1 h of reaction up to the end of the experiment.

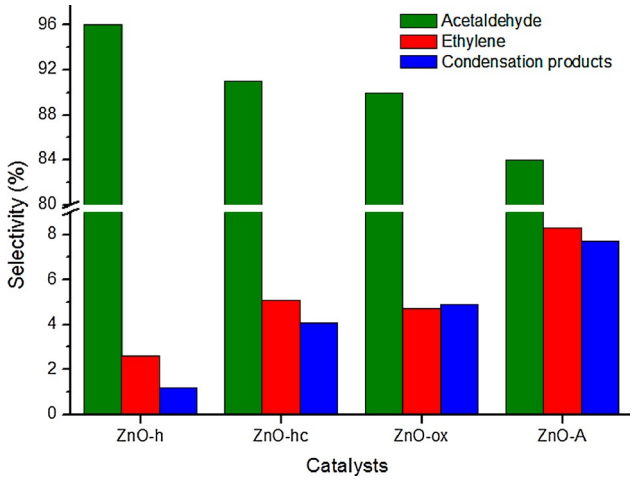

Figure 6. Selectivity catalytic results at 623 K for samples with similar (10$\bar{1}$0)/(0002) XRD peak intensity ratios. The results presented correspond to average values after 1 h of reaction up to the end of the experiment.

dissociation into an aldehyde intermediate and a hydride-like hydrogen atom that involves a neighboring acid site.[8a] Ethylene is formed mainly by the direct dehydration of ethanol over acid sites and does not undergo further reaction. However, acetaldehyde can undergo subsequent successive condensations, which is revealed by the continuous decrease of the acetaldehyde selectivity if the ethanol conversion increases, for instance, at high reaction temperatures (these experiments are not described for the sake of brevity). The main secondary product is ethyl acetate, which is obtained from the coupling of ethanol and acetaldehyde. For this, acetaldehyde is adsorbed on an acid site, and the hydrogen atom of the ethanol OH group is abstracted over surface basic sites to generate surface alkoxides. Thereafter, a hemiacetal is formed by the reaction of the surface alkoxide and the adsorbed aldehyde. The hemiacetal is dehydrogenated immediately to produce ethyl

acetate.[41] The other condensation product, 2-butenal, originates through a base-catalyzed aldol condensation mechanism (bimolecular reaction between adjacent adsorbed acetaldehyde species). In this case, the primary product is 3-hydroxybutanal, which is dehydrated easily to form 2-butenal over strong acid–base pairs.[9]

To test the stability of these catalysts and some deactivation phenomena under reaction conditions, all experiments were performed at 623 K for 6 h. For all ZnO samples, both the conversions and selectivities remained absolutely unaltered during our catalytic experiments. The values of specific activities and selectivities are average values taken after 1 h into the reaction up to the end of the each experiment. Finally, the determined specific activities are of the same order of magnitude, more precisely these values are: ZnO-E3, 2.0 $\mu mol\,m^{-2}\,s^{-1}$; ZnO-E4, 1.0 $\mu mol\,m^{-2}\,s^{-1}$; ZnO-ox, 1.2 $\mu mol\,m^{-2}\,s^{-1}$; ZnO-E5, 1.2 $\mu mol\,m^{-2}\,s^{-1}$; ZnO-h, 6.5 $\mu mol\,m^{-2}\,s^{-1}$; ZnO-hc, 1.7 $\mu mol\,m^{-2}\,s^{-1}$; and ZnO-A, 1.7 $\mu mol\,m^{-2}\,s^{-1}$.

As indicated in the previous section, the presence of surface sites of different natures and amounts on each sample can be related to their different morphologies. The obtained selectivities are presented for four catalysts as a function of the increased $(10\bar{1}0)/(0002)$ XRD intensity ratios in Figure 5. It is evident that the product distribution varies significantly with the catalyst studied. The formation of acetaldehyde decreases considerably with a catalyst that has a highly polar surface and, simultaneously, an increase in the selectivity to ethylene and condensation products occurs. ZnO-E3, which has a high proportion of nonpolar surfaces, exhibits the highest selectivity to acetaldehyde (94%), whereas the sample with the highest extent of basal surface, ZnO-E5, presents the lowest values (88%). These results highlight the requirement of the presence of nonpolar surfaces to optimize the dehydrogenation performance. Such a location of active sites is consistent with the work of Drouilly et al.,[11b] in which the high activity of this face is related to its high performance in the ethanol dehydrogenation reaction. However, as acetaldehyde is generally the main product observed even for the sample that exposes polar surfaces preferably, we cannot rule out the location of active acid–base Zn^{2+}–O^{2-} pairs involved in acetaldehyde formation on basal O-terminated $(000\bar{1})$ faces, as these could also expose surface acid–base pairs, which is supported by DFT calculations.[11b] With regard to ethylene selectivity, which increases gradually if the exposure of polar surfaces is maximized, the presence of Lewis acid Zn^{2+} sites on the (0001) surface and/or the oxygen vacancies on $(000\bar{1})$ surfaces might be responsible of the formation of this primary product. The selectivity towards ethylene over the needle-shaped sample ZnO-E5 is around four times higher than that with the brick-like sample ZnO-E3, which evidences the requirement of basal surfaces for ethylene formation. The increase in the selectivity to the secondary products ethyl acetate and 2-butenal with an increase in the $(10\bar{1}0)/(0002)$ intensity ratio is shown in Figure 5. Thus we can hypothesize that basal faces are also involved in these secondary condensation reactions.

In the case of samples with comparable $(10\bar{1}0)/(0002)$ intensity ratios, significant differences in the obtained selectivities are also found (Figure 6), even though these samples have a similar relative exposure of the different surfaces [$(10\bar{1}0)/(0002)$ intensity ratios of 1.27–1.31]. These findings led us to consider a parameter in addition to the morphology that controls the selectivity, as mentioned above for the first group of samples that display different $(10\bar{1}0)/(0002)$ intensity ratios. In the case of the second group of four samples, both the contribution of hydroxyl species at $\tilde{\nu} \approx 3400\ cm^{-1}$ (Figure 4b) and the isopropanol reaction test (Table 2) denote an increase in the acidic sites with moderate strength in the order: ZnO-h < ZnO-hc < ZnO-ox < ZnO-A. Selectivity values are presented for the different samples in the same order in Figure 6. Although the formation of acetaldehyde decreases, the selectivity to ethylene and condensation products increases. Thus, as reported in Figure 7, an increase in the density of acid sites caused by

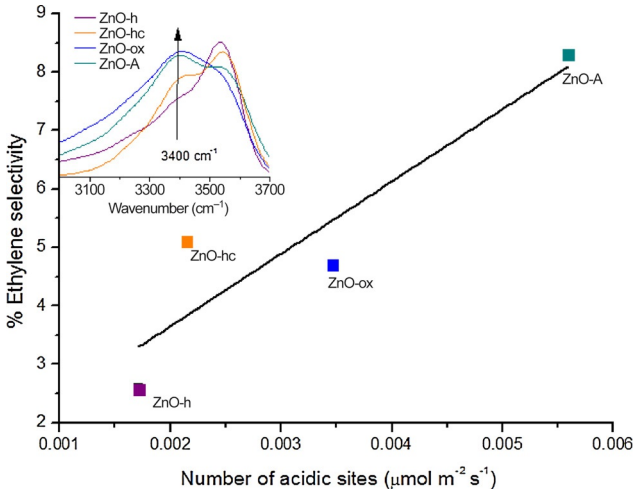

Figure 7. Ethylene selectivity as a function of the density of acidic hydroxyl groups determined from the isopropanol reaction test for ZnO samples with similar $(10\bar{1}0)/(0002)$ XRD peak intensity ratios.

these hydroxyl groups gives rise to an increase in the selectivity to ethylene. Previously, acidic hydroxyl groups have been described to act as active sites in the dehydrogenation of ethanol to ethylene in a series of commercial alumina materials.[42] The tendency caused by the effect of moderate acidic hydroxyl groups is also evident in the formation of secondary products (Figure 6), so we can propose that these types of hydroxyl groups act as acid active sites. From a catalytic point of view and under our experimental conditions, ZnO-A is able to produce yields of ethyl acetate six times higher than ZnO-h. It should be highlighted that these types of hydroxyl groups are related to polar surfaces, which evidences once again that active sites are different from one crystalline face to another. In other words, a surface-structure-sensitive phenomenon occurs.

Conclusions

A series of ZnO nanostructures prepared by different methods that display different morphologies and surface hydroxyl features have been tested in catalytic ethanol decomposition.

Characterization by XRD, SEM, diffuse reflectance infrared Fourier transform spectroscopy, and isopropanol decomposition allowed us to provide a complete structural, morphological, and superficial analysis of the materials. The interpretation of these results gave conclusive evidence on the key role played by the ratio of the polar and nonpolar facets exposed at the external surface of the ZnO nanomaterial on the studied reaction. It was shown that the maximization of specific activity is not obtained by maximizing the exposure of any particular type of surface (polar versus nonpolar) to the external solid surface. However, with regard to the selectivity, a structure-surface-sensitivity phenomenon was found in the ethanol decomposition: polar surfaces were more selective than nonpolar ones to minor products; ethylene and condensation products. Furthermore, it was determined that this dependence on morphology is related to the different superficial properties displayed by different types of surfaces. Specifically, the presence of particular acidic hydroxyl groups seems to be responsible for the acid catalytic properties that favor the formation of ethylene and condensation products, which evidences the indirect role of polar (or basal) surfaces on ZnO materials in the ethanol catalytic transformation. These results indicate the requirement to minimize the polar surface extension as well as the importance to control the acid–base properties in ZnO materials to optimize the dehydrogenation performance towards acetaldehyde as the main product.

Experimental Section

Three of the studied materials were prepared by a microemulsion method using *n*-heptane as the organic medium, Triton X-100 as the surfactant, and hexanol as the cosurfactant. The water/surfactant molar ratio was 9 (ZnO-E3), 6 (ZnO-E4), and 36 (ZnO-E5). Details are described in Ref. [26]. Three other samples were prepared as indicated in Ref. [43]. In brief, these were obtained by the thermal decomposition of zinc oxalate (ZnO-ox), zinc hydroxide (ZnO-h), and zinc hydroxicarbonate (ZnO-hc), respectively. A commercial sample Analar, from B.D.H. Chemicals Ltd, (ZnO-A) prepared by the combustion of Zn was also studied. All these samples were calcined at 723 K for 2 h before characterization and catalytic studies.

The catalysts were characterized as follows. The structural properties were determined by XRD by using a Rayflex XRD3100 instrument using with CuK_α X-rays ($\lambda = 1.54$ Å) and a Ni filter. Steps of 0.05° were employed with a time of 1 s per step and a 2θ range of 5–95°. The morphological appearance of the samples was observed by SEM by using a JEOL JSM 7600F system. Before observations by SEM, the samples were metalized to assure electron conduction. For this, a layer of Au with a thickness close to 5 nm was evaporated over each ZnO sample. Surface areas of the samples (S_{BET}) were measured from the adsorption of N_2 at 77 K by using an automatic volumetric adsorption apparatus (Micromeritics ASAP 2010) using the BET method. Before N_2 adsorption, the samples were outgassed for 8 h at 523 K.

DRIFTS spectra were collected by using a Varian 670 infrared spectrometer at 423 K under an Ar atmosphere. The spectra were obtained by collecting 200 scans with a resolution of 4 cm^{-1} and are presented in the absorbance mode. Furthermore, to gain information about the surface acid sites density with quantitative values, the samples were studied in the isopropanol dehydrogenation or dehydration test at 493 K. The experimental and the analytic system used in these reaction tests is the same that described below for the studies of ethanol valorization reactions. The mass of the catalyst was adjusted in each test to work under differential conditions (conversion values lower than 10%) in all cases.

The catalytic properties of the samples were studied for the transformation of ethanol in the gas phase at atmospheric pressure in a fixed-bed vertical microreactor (9 mm i.d.). Typically, a known mass of catalyst (with a particle size of 0.5–0.1 mm) was dispersed in solid-glass beads to increase the bed length and to avoid local heating. The reactor was placed inside a temperature-controlled heating jacket, and a thermocouple was placed at the centre of the catalytic bed. The catalytic experiments were performed at 623 K. Ethanol (99.5%, Panreac) was fed by using a micropump and vaporized in He (carrier gas). The resulting stream, 31 vol% of ethanol, was fed to the reactor at 20 $mL_{STP}\,min^{-1}$. The composition of the stream reactor effluents was analyzed on-line by GC (Varian CP-3800) with a Porapak Q column and equipped with flame ionization and thermal conductivity detectors.

The conversion was calculated using Equation (1):

$$X_{EtOH}(\%) = \frac{\sum_i n_i mol_i}{2mol_{EtOH} + \sum_i n_i mol_i} \cdot 100\% \quad (1)$$

in which n_i is the number of carbon atoms of the product i and mol_{EtOH} is the amount of unreacted ethanol in the stream reactor effluent.

The selectivity to a specific product was defined as follows [Eq. (2)]:

$$S_i(\%) = \frac{n_i mol_i}{\sum_i n_i mol_i} \cdot 100\% \quad (2)$$

Carbon mass balances in these catalytic tests were calculated as the ratio of the total composition of the stream reactor effluent (all formed products and unreacted ethanol) against the introduced ethanol, and resulted in all cases in an accuracy higher than 97%.

To discard the presence diffusion problems, the experiments performed were replicated with other particles sizes and with the double the catalyst weight. The results obtained suggest the absence of both external and internal mass transfer effects. Blank experiments were performed to verify the absence of catalytic activity under the conditions used in this study either with the empty reactor or filled with the glass beads. The catalyst properties in ethanol decomposition, conversions, and selectivities were unmodified during time on stream. These observations were extensive for all the samples with changes lower than 1% in both specific activity and selectivity values, which indicates clearly that the catalyst surfaces were quite stable under reaction conditions (no modifications of either the structure or chemical surface properties seem to occur).

Acknowledgements

The financial support of the Spanish government by Projects CTQ2011-29272-C04-01 and CTQ2011-29272-C04-03 is recognized. M.V.M. appreciates the financial support of UNED by a predoctoral grant. We thank the technical services of Universidad Complutense at Madrid for helping us in the SEM experiments.

Keywords: acidity · biomass · dehydrogenation · surface analysis · zinc

[1] a) G. A. Olah, *Angew. Chem. Int. Ed.* **2005**, *44*, 2636 – 2639; *Angew. Chem.* **2005**, *117*, 2692 – 2696; b) G. W. Huber, S. Iborra, A. Corma, *Chem. Rev.* **2006**, *106*, 4044 – 4098.
[2] a) A. Corma, S. Iborra, A. Velty, *Chem. Rev.* **2007**, *107*, 2411 – 2502; b) D. M. Alonso, J. Q. Bond, J. A. Dumesic, *Green Chem.* **2010**, *12*, 1493 – 1513; c) P. Gallezot, *Chem. Soc. Rev.* **2012**, *41*, 1538 – 1558.
[3] A. Birot, F. Epron, C. Descorme, D. Drupez, *Appl. Catal. B* **2008**, *79*, 17 – 25.
[4] a) J. A. Posada, A. D. Patel, A. Roes, K. Blok, A. P. C. Faaij, M. K. Patel, *Bioresour. Technol.* **2013**, *135*, 490 – 499; b) C. Angelici, B. M. Weckhuysen, P. C. A. Bruijnincx, *ChemSusChem* **2013**, *6*, 1595 – 1614.
[5] a) E. A. El-Katatny, S. A. Halawy, M. A. Mohamed, M. I. Zaki, *Appl. Catal. A* **2000**, *199*, 83 – 92; b) N. R. C. L. Machado, V. Calsavara, N. G. C. Astrath, U. K. Matsuda, A. Paesano, M. L. Baesso, *Fuel* **2005**, *84*, 2064 – 2070; c) V. Calsavara, M. L. Baesso, N. R. C. F. Machado, *Fuel* **2008**, *87*, 1628 – 1636; d) M. Almohalla, M. V. Morales, E. Asedegbega-Nieto, A. Maroto-Valiente, B. Bachiller Baeza, I. Rodríguez Ramos, A. Guerrero-Ruiz, *Open Catal. J.* **2014**, *7*, 1 – 7.
[6] E. Asedegbega-Nieto, M. Perez-Cadenas, M. V. Morales, B. Bachiller-Baeza, E. Gallegos-Suarez, I. Rodríguez-Ramos, A. Guerrero-Ruiz, *Diamond Relat. Mater.* **2014**, *44*, 26 – 32.
[7] F. W. Chang, H. C. Yang, L. S. Roselin, W. Y. Kuo, *Appl. Catal. A* **2006**, *304*, 30 – 39.
[8] a) T. Tsuchida, J. Kuboa, T. Yoshioka, S. Sakuma, T. Takeguchi, W. Ueda, *J. Catal.* **2008**, *259*, 183 – 189; b) M. León, E. Díaz, A. Vega, S. Ordoñez, A. Auroux, *Appl. Catal. B* **2011**, *102*, 590 – 599.
[9] M. León, E. Díaz, S. Ordoñez, *Catal. Today* **2011**, *164*, 436 – 442.
[10] M. Eckert, G. Fleischmann, R. Jira, H. M. Bolt, K. Golka in *Acetaldehyde. Ullmann's Encyclopedia of Industrial Chemistry*, Wiley-VCH, **2006**.
[11] a) S. A. Halawy, M. A. Mohamed, *J. Mol. Catal. A* **1995**, *98*, L63 – L68; b) C. Drouilly, J. M. Krafft, F. Averseng, H. Lauron-Pernot, D. Bazer-Bachi, C. Chizallet, V. Lecocq, G. Costentin, *Appl. Catal. A* **2013**, *453*, 121 – 129.
[12] a) S. Polarz, J. Strunk, V. Ischenko, M. W. E. van der Berg, O. Hinrichsen, M. Muhler, M. Driess, *Angew. Chem. Int. Ed.* **2006**, *45*, 2965 – 2969; *Angew. Chem.* **2006**, *118*, 3031 – 3035; b) J. Strunk, K. Kähler, X. Xia, M. Muhler, *Surf. Sci.* **2009**, *603*, 1776 – 1783.
[13] B. Meyer, D. Marx, O. Dulub, U. Diebold, M. Kunat, D. Langenberg, C. Wöll, *Angew. Chem. Int. Ed.* **2004**, *43*, 6641 – 6645; *Angew. Chem.* **2004**, *116*, 6809 – 6814.
[14] J. A. Rodriguez, A. Maiti, *J. Phys. Chem. B* **2000**, *104*, 3630 – 3638.
[15] T. Jirsak, J. Dvorak, J. A. Rodriguez, *J. Phys. Chem. B* **1999**, *103*, 5550 – 5559.
[16] O. Hinrichsen, K. Kochlöfl, M. Muhler in *Handbook of Heterogeneous Catalysis, 2nd ed.* (Eds.: G. Ertl, H. Knözinger, J. Weitkamp), Wiley-VCH, Weinheim, **2008**.
[17] Y. Wang, R. Kováčik, B. Meyer, K. Kotsis, D. Stodt, V. Stämmler, H. Qiu, F. Träger, D. Langenberg, M. Muhler, C. Wöll, *Angew. Chem. Int. Ed.* **2007**, *46*, 7315 – 7318; *Angew. Chem.* **2007**, *119*, 7456 – 7459.
[18] a) S. Gil Girol, T. Strunskus, M. Muhler, C. Wöll, *J. Phys. Chem. B* **2004**, *108*, 13736 – 13745; b) M. Messori, A. Vaccari, *J. Catal.* **1994**, *150*, 177 – 185.
[19] a) C. Richard, F. Bosquet, J. F. Pilichowski, *J. Photochem. Photobiol. A* **1997**, *108*, 45 – 49; b) M. D. Driessen, T. M. Miller, V. H. Grassian, *J. Mol. Catal. A* **1998**, *131*, 149 – 156; c) M. C. Yeber, J. Rodríguez, J. Freer, N. Durán, H. D. Mansilla, *Chemosphere* **2000**, *41*, 1193 – 1197.
[20] F. Viñes, A. Iglesias-Juez, F. Illas, M. Fernández-García, *J. Phys. Chem. C* **2014**, *118*, 1492 – 1505.
[21] B. Meyer, *Phys. Rev. B* **2004**, *69*, 045416.
[22] N. Kislov, J. Lahiri, H. Verma, D. Y. Goswanni, E. Stefanakos, M. Batzill, *Langmuir* **2009**, *25*, 3310 – 3315.
[23] T. Pauporte, J. Rathousky, *J. Phys. Chem. C* **2007**, *111*, 7639 – 7644.
[24] a) G. R. Li, T. Hu, G. L. Pan, T. Y. Yan, X. P. Gao, H. Y. Zhu, *J. Phys. Chem. C* **2008**, *112*, 11859 – 11864; b) Z. L. Wang, *ACS Nano* **2008**, *2*, 1987 – 1992.
[25] a) A. Mclaren, T. Valdes-Solis, G. Li, S. C. Tsang, *J. Am. Chem. Soc.* **2009**, *131*, 12540 – 12541; b) C. Lizandara-Pueyo, S. Siroky, M. R. Wagner, A. Hoffman, J. S. Reparaz, M. Lehmann, S. Polarz, *Adv. Funct. Mater.* **2011**, *21*, 295 – 304.
[26] A. Iglesias-Juez, F. Viñes, O. Lamiel-García, M. Fernández-García, F. Illas, *J. Mater. Chem. A* **2015**, *3*, 8782 – 8792.
[27] J. C. Védrine, *Appl. Catal. A* **2014**, *474*, 40 – 50.
[28] M. Boudart, *Adv. Catal.* **1969**, *20*, 153 – 166.
[29] J. C. Volta, W. Desquesnes, B. Moraweck, G. Coudurier, *React. Kinet. Catal. Lett.* **1979**, *12*, 241 – 246.
[30] H. Wilmer, M. Kurtz, K. V. Klementiev, O. P. Thachenko, W. Grünert, O. Hinrichsen, A. Birkner, S. Rabe, K. Merz, M. Driess, C. Wöll, M. Muhler, *Phys. Chem.* **2003**, *2*, 4736 – 4742.
[31] a) J. M. Vohs, M. A. Barteau, *J. Phys. Chem.* **1987**, *91*, 4766 – 4776; b) J. M. Vohs, M. A. Barteau, *Surf. Sci.* **1988**, *201*, 481 – 502; c) J. M. Vohs, M. A. Barteau, *Surf. Sci.* **1988**, *197*, 109 – 122.
[32] O. Dulub, U. Diebold, G. Kresse, *Phys. Rev. Lett.* **2003**, *90*, 016102.
[33] S. A. French, A. A. Sokol, S. T. Bromley, C. R. A. Catlow, P. Sherwood, *Top. Catal.* **2003**, *24*, 161 – 172.
[34] H. Noei, H. Qiu, Y. Wang, M. Mühler, C. Wöll, *ChemPhysChem* **2010**, *11*, 3604 – 3607.
[35] a) C. Chizallet, H. Petitjean, G. Costentin, H. Lauron-Pernot, J. Maquet, C. Bonhomme, M. Che, *J. Catal.* **2009**, *268*, 175 – 179; b) H. Petitjean, J. M. Krafft, M. Che, H. Lauron Pernot, G. Costentin, *Phys. Chem. Chem. Phys.* **2010**, *12*, 14740 – 14748.
[36] a) E. Angelescu, O. D. Pavel, M. Che, R. Birjega, G. Constentin, *Catal. Commun.* **2004**, *5*, 647 – 651; b) F. Winter, X. Xia, B. P. C. Hereijgers, J. H. Bitter, A. J. van Dillen, M. Muhler, K. P. de Jong, *J. Phys. Chem. B* **2006**, *110*, 9211 – 9218; c) J. Roelofs, D. Lensveld, A. V. Dillen, K. D. Jong, *J. Catal.* **2001**, *203*, 184 – 191.
[37] A. Patterson, *Phys. Rev.* **1939**, *56*, 978 – 982.
[38] C. Lamberti, A. Zecchina, E. Groppo, S. Bordiga, *Chem. Soc. Rev.* **2010**, *39*, 4951.
[39] a) H. Noei, H. Qiu, Y. Wang, E. Löffler, C. Wöll, M. Mühler, *Phys. Chem. Chem. Phys.* **2008**, *10*, 7092 – 7097; b) R. P. Eischens, W. A. Pliskin, M. J. D. Low, *J. Catal.* **1962**, *1*, 180 – 191; c) F. Boccuzzi, E. Borello, A. Zecchina, A. Bossi, M. Camia, *J. Catal.* **1978**, *51*, 150 – 159; d) G. L. Griffin, J. T. Yates, *J. Chem. Phys.* **1982**, *77*, 3744 – 3750.
[40] A. Gervasini, J. Fenyvesi, A. Auroux, *Catal. Lett.* **1997**, *43*, 219 – 228.
[41] K. Inui, T. Kurabayashi, S. Sato, N. Ichikawa, *J. Mol. Catal. A* **2004**, *216*, 147 – 156.
[42] T. K. Phung, A. Lagazzo, M. A. Rivero-Crespo, V. Sánchez-Escribano, G. Busca, *J. Catal.* **2014**, *311*, 102 – 114.
[43] A. Guerrero-Ruiz, I. Rodriguez-Ramos, *ACS Symp. Ser.* **1996**, *638*, 347 – 353.

Received: March 25, 2015
Revised: April 27, 2015
Published online on June 18, 2015